RhoGEF Tiam2 Regulates Glutamatergic Synaptic Transmission in Hippocampal CA1 Pyramidal Neurons

Sadhna Rao, Feng Liang, and Bruce E. Herring

Department of Biological Sciences, Neurobiology Section, Dornsife College of Letters, Arts and Sciences, University of Southern California, Los Angeles, California 90089

Abstract

Glutamatergic synapses exhibit significant molecular diversity, but circuit-specific mechanisms that underlie synaptic regulation are not well characterized. Prior reports show that Rho-guanine nucleotide exchange factor (RhoGEF) Tiam1 regulates perforant path→dentate gyrus granule neuron synapses. In the present study, we report Tiam1's homolog Tiam2 is implicated in glutamatergic neurotransmission in CA1 pyramidal neurons. We find that Tiam2 regulates evoked excitatory glutamatergic currents via a postsynaptic mechanism mediated by the catalytic Dbl-homology domain. Overall, we present evidence for RhoGEF Tiam2's role in glutamatergic synapse function at Schaffer collateral→CA1 pyramidal neuron synapses.

Key words: development; glutamatergic; hippocampus; regulation; spines; synapse

Significance Statement

Glutamatergic synapses are known to vary in composition and function, but how this heterogeneity is established to create input-specific synaptic diversity is not well understood. In the present study, we show Tiam2 regulates glutamatergic neurotransmission at Schaffer collateral→CA1 pyramidal neuron synapses. We find that this function is dependent on its catalytic domain. By contrast we did not observe a role for Tiam2 in synaptic transmission at perforant path→DG granule neuron synapses. We also find that Tiam1 and Tiam2 are individually dispensable for functional synaptic plasticity in CA1 pyramidal neurons. To our knowledge, this is the first evidence of the Rho-guanine nucleotide exchange factor Tiam2's role in regulating glutamatergic synapses.

Introduction

Recent studies have highlighted the molecular heterogeneity of glutamatergic synapses (Wichmann and Kuner, 2022). Transcriptomic and proteomic profiling has revealed cell type- and input-specific diversity in synaptic molecular composition (Zhao et al., 2001; Fort and Blangy, 2017; Zhu et al., 2018; Farris et al., 2019; Gerber et al., 2019; Franjic et al., 2022). However, an understanding of how synapse maturation, circuit assembly, and plasticity are regulated by distinct synaptic proteomes presents a significant challenge (Gutman-Wei and Brown, 2021; Marcassa et al., 2023).

Rho-guanine nucleotide exchange factors (RhoGEFs) are widely implicated in molecular mechanisms essential to the assembly and function of glutamatergic synapses (Kang and Schuman, 1995; Penzes et al., 2001, 2003; Fu et al., 2007; Margolis et al., 2010; Herring and Nicoll, 2016; Hamilton et al., 2017; Martin-Vilchez et al., 2017). RhoGEFs contain a catalytic Dbl-homology (DH) domain that catalyzes small-GTPase activity and promotes actin polymerization within postsynaptic compartments (Karnoub et al., 2001; Miller et al., 2013). Previous work has shown that the RhoGEF Tiam1 is important for

the function of glutamatergic synapses at perforant path→dentate gyrus (DG) granule neuron synapses (Rao et al., 2019; Cheng et al., 2021). In the present study, we describe a functional role of the homologous protein Tiam2 at Schaffer collateral–CA1 pyramidal neurons.

Previous reports have characterized Tiam2's role in cell migration and neurite extension in vitro (Matsuo et al., 2002; Yoshizawa et al., 2002; Chan et al., 2020). We find that shRNA-mediated depletion of Tiam2 in CA1 pyramidal neurons results in significant reductions in AMPA receptor (AMPAR)- and NMDA receptor (NMDAR)-mediated evoked currents. We establish that postsynaptic Tiam2 expression contributes to glutamatergic neurotransmission and that Tiam2's effect on neurotransmission at Schaffer collateral→CA1 pyramidal neuron synapses depends on its catalytic DH1 domain. Tiam1 shares significant DH1 domain homology with Tiam2, and we show that recombinant Tiam1 expression can readily substitute for Tiam2 in supporting glutamatergic neurotransmission at this synapse. Additionally, our data also suggest no role for Tiam2 in neurotransmission at perforant path→DG granule neuron synapses. Moreover, we find that Tiam1 and Tiam2 are individually dispensable for functional long-term potentiation (LTP) at Schaffer collateral→CA1 pyramidal neuron synapses. In summary, we find that Tiam2 regulates baseline glutamatergic neurotransmission at Schaffer collateral→CA1 pyramidal neuron synapses.

Materials and Methods

Experimental constructs. A previously characterized Tiam2 shRNA target sequence against rat Tiam2 was used (5′-GGAGCTGCCTTTCTCACTTTA-3; Goto et al., 2011). The Tiam2 shRNA was subcloned behind the H1 promoter region of a GFP-expressing pFHUGW expression vector. A single-nucleotide mismatch was identified in the corresponding mouse Tiam2 target sequence. However, Western blot analysis confirmed effective and specific knockdown of Tiam2 expression by the rat-directed shRNA in both rat and mouse neurons (Fig. 1B and Extended Data Fig. 4-1B,C).

All cloning was performed using overlap-extension PCR followed by In-Fusion Cloning (Clontech Laboratories). The shRNA-resistant Tiam2 was generated by introducing five silent-point mutations within the RNAi target sequence in Tiam2 cDNA (GAAGTTGTCTATCACACTTTA). Tiam1 cDNA was from Horizon Discovery (catalog #MHS6278-211691099), and Tiam2 cDNA was from GenScript Biotech (catalog #ORa14059). cDNA sequences were cloned into pCAGGS-IRES-mCherry expression vectors. The Tiam2 ΔDH mutant was generated by deletion of the ~200-residue DH1 domain (Arg1117-Met1312) using overlap-extension PCR followed by In-Fusion Cloning (Clontech Laboratories) into a pCAGGS-IRES-mCherry expression vector. Expression constructs were coexpressed with a pFHUG vector containing GFP, which also served as a control vector for spine imaging experiments.

Tissue harvest and immunohistochemistry. All animal procedures were performed in accordance with the University of South California animal care committee's regulations. Postnatal Day (P) 15 rats were perfused with 4% paraformaldehyde via transcardial perfusion following which hippocampi were dissected and fixed in 4% PFA overnight at 4°C and then transferred into 1XPBS solution. Fixed tissue was sliced to 100–150 μm slices using a MX-TS tissue slicer (Siskiyou). Tissue sections were probed with antibodies (mouse monoclonal anti-Tiam2, 1:100, sc-514090, Santa Cruz Biotechnology; sheep anti-Tiam1, 1:100 AF5038, R&D Systems; and anti-Prox1, 1:2000, ab5475, Merck Millipore). For peptide control experiments, antibody was incubated with a blocking peptide (sc-514090 P) at 1:1 ratio overnight at 4°C and applied to samples in parallel with antibody staining. Fluorophore-coupled secondary antibodies were used for antibody detection, and slides were imaged using a Zeiss LSM-780 inverted microscope equipped with a 10×/0.45 M27 objective. Tiled 16-bit images were processed using Zen (Zeiss) to produce a single image file.

Organotypic slice preparation and electrophysiology. P6 to P8 Sprague Dawley rats of both sexes were used to prepare organotypic hippocampal slice cultures as previously described (Stoppini et al., 1991; Prang et al., 2001; Bonnici and Kapfhammer, 2009). Hippocampal tissue with and without attached entorhinal cortical tissue were harvested from six to eight rat pups, and an MX-TS tissue slicer (Siskiyou) was used to prepare

Correspondence should be addressed to Sadhna Rao at raos27@gene.com or Bruce E. Herring at bherring@usc.edu.
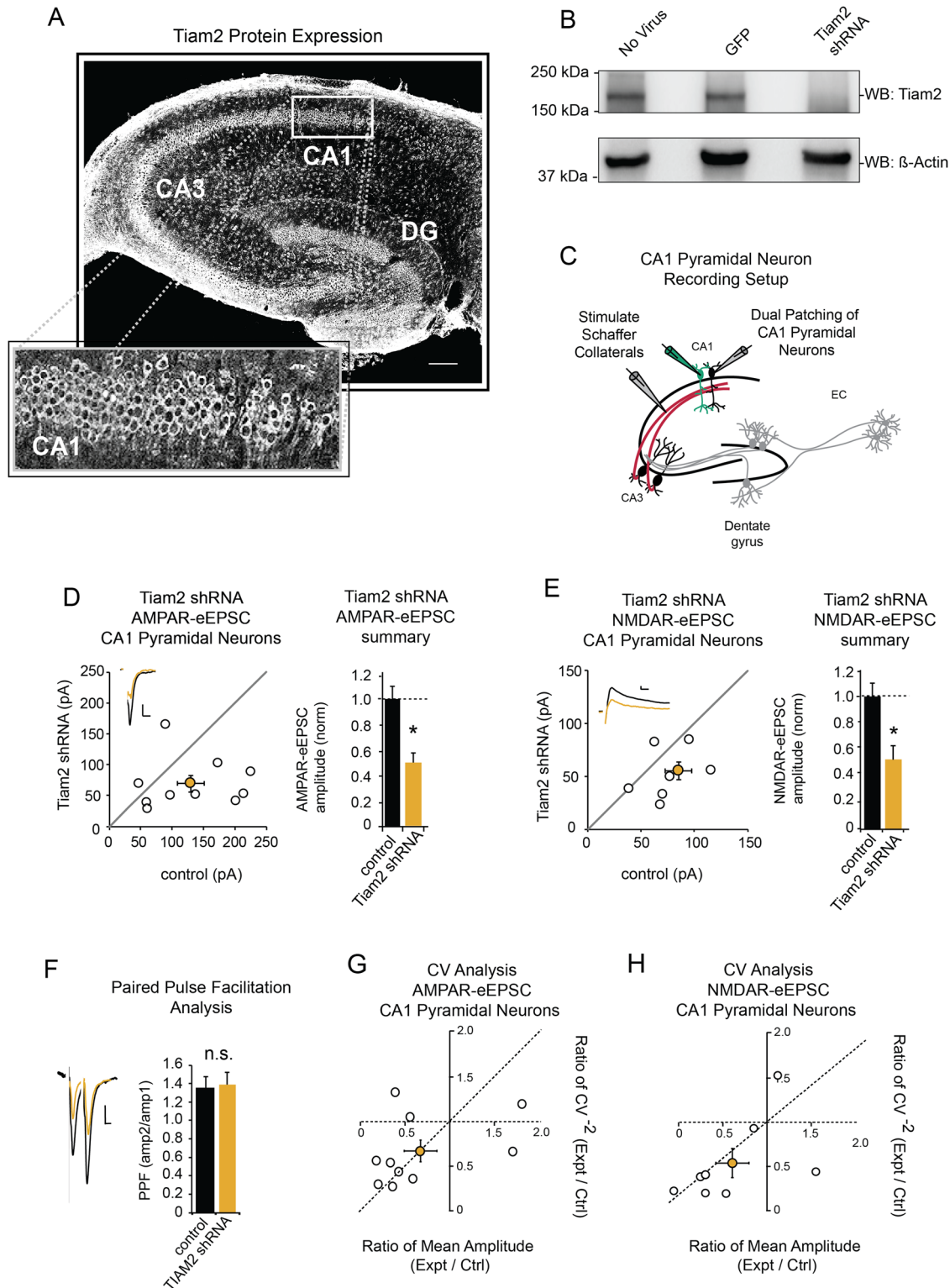
Figure 1. Tiam2 knockdown reduces baseline AMPAR- and NMDAR-mediated neurotransmission in CA1 pyramidal neurons. ***A***, Tiam2 immunolabeling in whole hippocampal slice, (inset) CA1 cell body layer (scale bar, 200 μm). ***B***, Western blot showing shRNA-mediated reduction of Tiam2 expression in dissociated rat hippocampal neurons. ***C***, Schematic representation of electrophysiological recording setup for CA1 pyramidal neurons. ***D***, ***E***, Scatterplots show eEPSC amplitudes for pairs of untransfected and transfected cells (open circles) with $M \pm$ SEM (filled circles). (Insets) Representative current traces from control (black) and transfected (yellow) neurons with stimulation artifacts removed (scale bars: 20 pA for both AMPAR-eEPSCs and NMDAR-eEPSCs, 20 ms for AMPAR, 50 ms for NMDAR). Barplots show average AMPAR and NMDAR-eEPSC amplitudes (±SEM) of CA1 pyramidal neurons expressing Tiam2 shRNA (yellow) normalized to their respective control cell average eEPSC amplitudes (black). Tiam2 shRNA expression decreases AMPAR-eEPSC and NMDAR-eEPSC amplitude in CA1 pyramidal neurons ($p = 0.048$; $n = 10$ pairs for AMPAR-eEPSC; $p = 0.038$; $n = 8$ pairs for

400 μm transverse sections. Tissue slices were placed on squares of Biopore Membrane Filter Roll (Merck Millipore, catalog #BGCM00010) and placed on Millicell Cell Culture inserts (Merck Millipore) in 35 mm dishes containing 1 ml culture media (MEM + HEPES, Invitrogen 12360-038, 25% horse serum, 25% HBSS, and 1 mM L-glutamine). Media were replaced on alternate days.

Biolistic transfections were performed on DIV1 as previously described (Stoppini et al., 1991; Schnell et al., 2002; W. Lu et al., 2009). Briefly, 1-μm-diameter gold particles were coated with 50 μg plasmid DNA via coprecipitation with $CaCl_2$, serially washed with ethanol. DNA-coated gold particles were coated onto the inner surface of PVC tubing, dried using nitrogen gas, and used for DNA delivery with a Helios Gene Gun (Bio-Rad Laboratories). Recordings were made on DIV 7 or 9 in organotypic slice cultures at room temperature (RT). The recording chamber was perfused at 2.5 ml/min^{-1} with artificial cerebrospinal fluid (aCSF) containing 119 mM NaCl, 2.5 mM KCl, 1 mM NaH_2PO_4, 26.2 mM $NaHCO_3$, and 11 mM glucose bubbled with 95% (v/v) O_2 and 5% (v/v) CO_2 to maintain pH. aCSF was supplemented with 4 mM $CaCl_2$ and 4 mM $MgSO_4$. Five micromolar 2-chloroadenosine was added to dampen epileptiform activity and 0.1 mM picrotoxin to block GABA (A) receptors. Osmolality was adjusted to 305–315 mOsm. Borosilicate glass recording pipettes were filled with a pipette internal solution suited for whole-cell recordings buffered at 7.3–7.4 pH and composed of the following (in mM): 135 $CsMeSO_4$, 8 NaCl, 10 HEPES, 0.3 EGTA, 5 QX-314, 4 Mg-ATP, and 0.3 Na-GTP.

All electrophysiology experiments were performed on an upright Olympus BX50WI microscope. Differential interference phase contrast microscopy was used to identify untransfected DG granule neurons and CA1 pyramidal neurons, while GFP-transfected cells were identified using epifluorescence microscopy. Stratum radiatum pathway and perforant pathway afferents were stimulated with a monopolar glass electrode to produce simultaneous postsynaptic currents measured from a pair of untransfected and transfected CA1 pyramidal and DG granule neurons, respectively. This approach allows for a pairwise, internally controlled comparison of the consequences of acute genetic manipulations in the transfected postsynaptic neuron (Arnold and Heintz, 1997; McAllister, 2004; Pfeiffer et al., 2010; Rao et al., 2019). Membrane voltage was held at −70 mV to measure AMPAR-evoked excitatory postsynaptic currents (eEPSCs) and at +40 mV to measure NMDAR-eEPSCs. NMDAR current amplitudes were measured at 150 ms after stimulation to avoid contamination from AMPAR current. AMPAR- and NMDAR-mediated currents were typically recorded from the same cell. Paired-pulse facilitation was induced by delivery of two consecutive stimuli at intervals of 20 ms. No more than one pair was recorded from a single hippocampal slice. Membrane-holding current, pipette series resistance, and input resistance were monitored throughout recording sessions. Data were gathered through a MultiClamp 700B amplifier (Axon Instruments), filtered at 2 kHz, and digitized at 10 kHz.

Acute slice preparation and LTP. For acute slice experiments, in utero electroporation was performed as previously described (Elias et al., 2008). P18–P24 mice were subjected to isoflurorane exposure and verified to be under a surgical plane of anesthesia. Three hundred micrometer transverse slices were cut from a freshly harvested hippocampus using a ZERO1 vibrating microtome (Ted Pella). Slices were collected in cold high-sucrose low–sodium cutting solution containing the following (in mM), 2.5 KCl, 0.5 $CaCl_2$, 7 $MgCl_2$, 1.25 NaH_2PO_4, 25 $NaHCO_3$, 7 glucose, 210 sucrose, and 1.3 ascorbic acid, bubbled with 95% O_2 and 5% CO_2. Thereafter slices were transferred to aCSF but supplemented with $CaCl_2$ at 2.5 mM and $MgSO_4$ at 1.3 mM with osmolality adjusted to 290–295 mM. Slices were incubated in aCSF saturated with 95% O_2 and 5% CO_2 at 37°C and RT for 40 min each after which slices were transferred to the recording chamber maintained in oxygenated aCSF. Borosilicate recording pipettes were filled with the same internal solution as organotypic slices. To minimize runup of baseline responses during LTP, cells were held cell attached for ∼1–2 min before breaking into the cell. GFP-transfected neurons were held at −70 mV in whole-cell configuration, while a borosilicate pipette filled with aCSF was used to stimulate Schaffer collateral afferents in the stratum radiatum. Baseline individual synaptic responses were measured for ∼2 min. Thereafter, LTP was induced within 5 min of achieving the whole-cell configuration by holding neurons at 0 mV during a 2 Hz stimulation of Schaffer collateral afferents for 90 s.

Imaging and spine analysis. Cultured hippocampal slices were transfected with pFHUGW-GFP shRNA constructs alone or pFHUGW-GFP shRNA and pCAGGS-mCherry cDNA constructs ∼18–20 h after plating using biolistic transfection. The experimenter was blinded to the genotype during subsequent processing and imaging. Slices were fixed in 4% PFA, 4% sucrose in 1× PBS, and washed with 1× PBS and then cleared with an abbreviated SeeDB-based protocol and mounted on microscope slides (Ke et al., 2013). High-resolution confocal Z-stacks of spine-containing CA1 pyramidal neuron apical dendrites were acquired on a Zeiss 510 microscope using a Plan Apochromat 40×/1.4 Oil DIC objective.

←

NMDAR-eEPSC; Wilcoxon signed-rank test). **F**, Paired-pulse facilitation ratio ($M \pm$ SEM) for Tiam2 shRNA expressing CA1 pyramidal neurons and paired control neurons with no detectable difference in facilitation ($p = 0.88$; $n = 5$ pairs; Student's unpaired t test). Representative scaled current traces from control and transfected (yellow) neurons (scale bars: 20 pA, 20 ms). **G**, **H**, CV analysis of AMPAR- and NMDAR-eEPSCs from pairs of control and Tiam2 shRNA expressing CA1 pyramidal neurons. CV^{-2} values are plotted against corresponding ratios of M amplitudes within each pair (open circles) with $M \pm$ SEM (filled circle; for AMPAR-eEPSCs, $n = 10$ pairs; for NMDAR-eEPSC, $n = 8$ pairs,). *$p < 0.05$, n.s., not significant. See Extended Data Figure 1-1 for more details.

Z-stacks were collected at 2,048 px × 2,048 px, 16-bit *X-Y* pixel dimensions, with *X-Y* spatial resolution of 70 nm and axial resolution of 500 nm with a 488 nm laser excitation wavelength. Automated analysis of dendritic segments and spines was performed using the commercially available software Filament Tracer (Imaris 9.1.2, Bitplane). For each cell, an ~60 μm dendritic segment was manually selected for analysis, and thresholds for dendritic surface and spine rendering were set (10 μm dendrite length; minimum spine diameter and maximum spine length were set to 0.2 and 2 μm, respectively). Data were exported into Microsoft Excel and analyzed and graphed using R Studio (Version 1.1.153).

Lentivirus preparation. Lentivirus was generated by transfecting HEK293T cells with plasmids pVSV-G and psPAX2 along with shRNA expressing constructs using FuGENE HD transfection reagent (Roche). Viral particle containing supernatant was collected 48 h later. Supernatant was filtered at 70 μm, concentrated using PEG-it (System Biosciences). Then viral particles were pelleted via centrifugation and resuspended in DMEM.

Western blotting. Embryonic Day (E)16.5 rat or mouse hippocampi were dissected, dissociated, and cultured in DMEM with 10% FBS. Neurons were plated onto six-well plates and infected with 20 μl virus (pFHUG-IRES-GFP lentivirus or pFHUG-Tiam2-shRNA-IRES-GFP lentivirus). At DIV 21, cell lysates were prepared and run on a 4–15% Mini-PROTEAN TGX Precast Protein Gel (Life Technologies) with 25–50 μg of protein loaded per lane. For experiments involving the expression of constructs in HEK293T cells (ATCC), cells seeded in six-well plates were transfected with 2 μg of total DNA, and lysates were prepared after 72 h of expression. Membranes were probed with antibodies specific for Tiam2 (1:100; sc-514090, Santa Cruz Biotechnology, and ab199426, Abcam), Tiam1 (1:100; sc-393315, Santa Cruz Biotechnology), and β-actin [1:1000, (13E5) Rabbit mAb 4970, Cell Signaling Technology]. Horseradish peroxidase-conjugated secondary antibodies were used for chemiluminescent detection. Membranes were scanned using Bio-Rad ChemiDoc MP Imaging System and exported using Image Lab Software.

Experimental design and data analysis. For all experiments, at least three male and three female rat pups were used. Imaging analysis was performed blind to genotype. All electrophysiological data are expressed as mean (M) ± standard error measurement (SEM). Data from simultaneous dual whole-cell recordings are shown within scatterplots, wherein each open circle represents one paired recording and a closed circle represents the average of all paired recordings. If the average data point falls above the diagonal line, it indicates that the eEPSC is lower in the control neuron and vice versa. Paired-pulse facilitation was calculated by dividing the peak response from the second stimulus by the peak response of the first stimulus.

Statistical significance was determined using Wilcoxon signed-rank test for paired dual whole-cell patch–clamp data, Wilcoxon rank-sum test for imaging data, and Student's *t* test for paired-pulse facilitation data. All *p* values <0.05 were considered significant and denoted with a single asterisk, *p* values <0.01 were denoted with a double asterisk, and *p* values <0.001 were denoted with a triple asterisk. All error bars represent standard error measurement. Sample sizes in the present study are as reported previously (Herring and Nicoll, 2016; Incontro et al., 2018).

Coefficient of variation (CV) analysis was performed by calculating the M and standard deviation (SD) of AMPAR-eEPSCs (Kokaia et al., 1998). At least 20 consecutively recorded current amplitudes for both control and transfected cells within a paired dual whole-cell patch–clamp recording were used to obtain the CV, calculated as SD/M. Theoretical and experimental work has shown that CV^{-2} (M^2/SD^2) is invariant with changes in the quantal size (i.e., the number of AMPA receptors at all synapses) and that CV^{-2} varies predictably with changes in the quantal content (i.e., the number of functional synapses containing AMPA receptors) according to the following equation $CV^{-2} = n \times P_r/(1 - P_r)$ where n is the number of vesicle release sites and P_r is the probability of presynaptic release. To observe the eEPSC variance with changes in the mean amplitude, the CV^{-2} values for transfected and control cells were plotted on the *y*-axis, and the ratios of means for transfected and control cells were plotted on the *x*-axis. Values above the 45° ($y = x$) line indicate increases in quantal content, while values approaching the horizontal line ($y = 1$) indicate a change in the quantal size as ultimately responsible for the difference in AMPAR-eEPSC amplitude between the control and transfected cells. For LTP, individual experiments were normalized to the baseline (before stimulation), and 12 consecutive responses were averaged to generate 1 min bins, which were then averaged to generate summary graphs. Bar graphs of LTP are averaged eEPSC values for the first 2 min (prior to LTP induction) and last 2 min of LTP summary graphs. For immunoblotting experiments, images are representative of three experimental replicates. For quantification, proteins were transferred to the same nitrocellulose membrane and probed in parallel for technical consistency. Background-adjusted band intensities were measured on Image Lab (Bio-Rad Laboratories), graphed on GraphPad Prism, and analyzed for statistical significance using the Mann–Whitney test.

Results

Tiam2 knockdown produces significant reductions in AMPAR- and NMDAR-mediated neurotransmission at CA1 pyramidal neurons

Immunostaining of rat hippocampal slices revealed robust Tiam2 expression throughout the hippocampal formation (Fig. 1*A*; Extended Data Fig. 1-1*A*) consistent with reports of Tiam2 mRNA expression (Zhao et al., 2001; Lein et al.,

2007; Cembrowski et al., 2016). To determine whether Tiam2 regulates glutamatergic neurotransmission in CA1 pyramidal neurons, we utilized a shRNA (Goto et al., 2011) that depletes Tiam2 protein expression (Fig. 1B; Extended Data Fig. 1-1B). We biolistically transfected rat hippocampal slices with Tiam2 shRNA and simultaneously recorded currents in transfected and untransfected CA1 pyramidal neurons evoked by Schaffer collateral stimulation (Fig. 1C). Our measurements of AMPAR- and NMDAR-mediated eEPSCs revealed a substantial ∼50 and ∼40% reduction in AMPAR-eEPSCs and in NMDAR-eEPSCs amplitudes, respectively (Fig. 1D,E). This is in contrast to the homolog Tiam1, whose depletion produced no observable effect of glutamatergic neurotransmission in CA1 pyramidal neurons (Rao et al., 2019).

To examine whether Tiam2's impact on glutamatergic neurotransmission is the result of presynaptic mechanism, we performed an analysis of paired-pulse facilitation at Schaffer collateral→CA1 pyramidal neuron synapses. We found that loss of Tiam2 protein expression in CA1 pyramidal neurons had no effect on paired-pulse facilitation (Fig. 1F), indicating presynaptic neurotransmitter release mechanisms are unaltered and Tiam2's role in supporting glutamatergic synapse function is postsynaptic.

Tiam2 knockdown reduces spine density in CA1 pyramidal neurons

Next, we determined the synaptic alteration underlying reductions in AMPAR- and NMDAR-eEPSC amplitudes following Tiam2 knockdown. These alterations could arise from uniform reduction in postsynaptic AMPARs and NMDARs across all glutamatergic synapses or loss of a subset of functional glutamatergic synapses in CA1 pyramidal neurons. We performed CV^{-2} analysis, with a comparison of the normalized variance of eEPSC amplitudes from two neurons receiving the same stimulus to identify changes in the quantal size and/or quantal content (Del Castillo and Katz, 1954; Bekkers and Stevens, 1990; Malinow and Tsien, 1990; Gray et al., 2011; Levy et al., 2015). Data points that lie on the horizontal dotted line indicate changes in the quantal size and represent uniform changes in receptor function across existing synapses. Data points that fall on or near the diagonal dotted line indicate changes in the quantal content and represent changes in the number of functional glutamatergic synapses (Bekkers and Stevens, 1990; Malinow and Tsien, 1990). The averages for both AMPAR and NMDAR excitatory currents fell on or near the diagonal dotted line (Fig. 1G,H), showing that deficits in current amplitudes are explained by changes in quantal content. Thus, reductions in AMPAR- and NMDAR-eEPSC amplitude following Tiam2 knockdown result from a reduced number of functional glutamatergic synapses.

Tiam2 catalyzes small-GTPase Rac1 activity, which promotes actin-dependent formation of dendritic spines (Tashiro and Yuste, 2004; Goto et al., 2011). Similar reductions in AMPAR- and NMDAR-eEPSC amplitudes and CV^{-2} analysis suggest an underlying reduction in dendritic spine density. We compared Tiam2 shRNA- and GFP-transfected CA1 pyramidal neurons (Fig. 2A) and observed a dramatic loss in the spine number relative to control neurons (Fig. 2B,C). Spine length and other parameters remained unchanged (Fig. 2C; Extended Data Fig. 2-1A–D). We verified that reduced AMPAR and NMDAR function produced by Tiam2 knockdown could be rescued by recombinant Tiam2 expression. To do this we coexpressed Tiam2 shRNA and a recombinant shRNA-resistant Tiam2 cDNA in CA1 pyramidal neurons and recorded AMPAR- and NMDAR-eEPSCs. We found that AMPAR- and NMDAR-eEPSC amplitudes were similar between control and transfected neurons, demonstrating Tiam2 cDNA was sufficient to rescue Tiam2 knockdown (Fig. 2D,E). The expression of Tiam2 cDNA was also sufficient to rescue deficits in spine density in CA1 pyramidal neuron dendrites (Fig. 2F–H; Extended Data Fig. 2-1E–H). These results further demonstrate that Tiam2 shRNA is specific for endogenous Tiam2, and the loss-of-function phenotypes we observe are a result of targeted reduction in Tiam2 protein expression. Moreover, the reduction in dendritic spine density corroborates our previous functional analyses and is consistent with Tiam2's role in supporting glutamatergic synapse structure and function in CA1 pyramidal neurons.

Tiam2 has a DH1 domain-dependent role in neurotransmission at Schaffer collateral–CA1 pyramidal neurons and is dispensable for baseline neurotransmission at perforant path–DG granule neurons

The DH1 domain mediates actin polymerization via Rac1 (Fig. 3A; Zheng et al., 1996; Worthylake et al., 2000; Karnoub et al., 2001). We verified that DH1 domain-lacking recombinant Tiam2 ΔDH (Fig. 3A) has expression comparable to wild-type Tiam2 in HEK293T cells (Fig. 3B). We found that CA1 pyramidal neurons expressing Tiam2 ΔDH and Tiam2 shRNA showed a ∼60 and ∼40% reduction in AMPAR- and NMDAR-eEPSC amplitudes, respectively (Fig. 3C,D), which is comparable to reductions resulting from shRNA-mediated Tiam2 knockdown. These data confirm that the DH1 domain is necessary for Tiam2's role in neurotransmission at Schaffer collateral–CA1 pyramidal neurons.

Tiam2 has significant expression in DG granule neurons (Fig. 1A). Surprisingly, we found that Tiam2 depletion in DG granule neurons had no effect on AMPAR and NMDAR current amplitude (Fig. 3F,G), with no alterations in spine morphology (Extended Data Fig. 3-1A–C). This suggests a DH1-dependent role of Tiam2 at Schaffer collateral→CA1 pyramidal neurons and no role for Tiam2 in neurotransmission at perforant path→DG granule neuron synapses.

Tiam1 and Tiam2 are individually dispensable for functional LTP in CA1 pyramidal neurons

Although Tiam1 and Tiam2 have similar domains, they display distinct ligand specificities in vitro (Shepherd et al., 2011). Tiam2 shares 71% of DH1 domain identity with Tiam1 (Fig. 4A; Chiu et al., 1999; Hoshino et al., 1999; Cook et al., 2014).
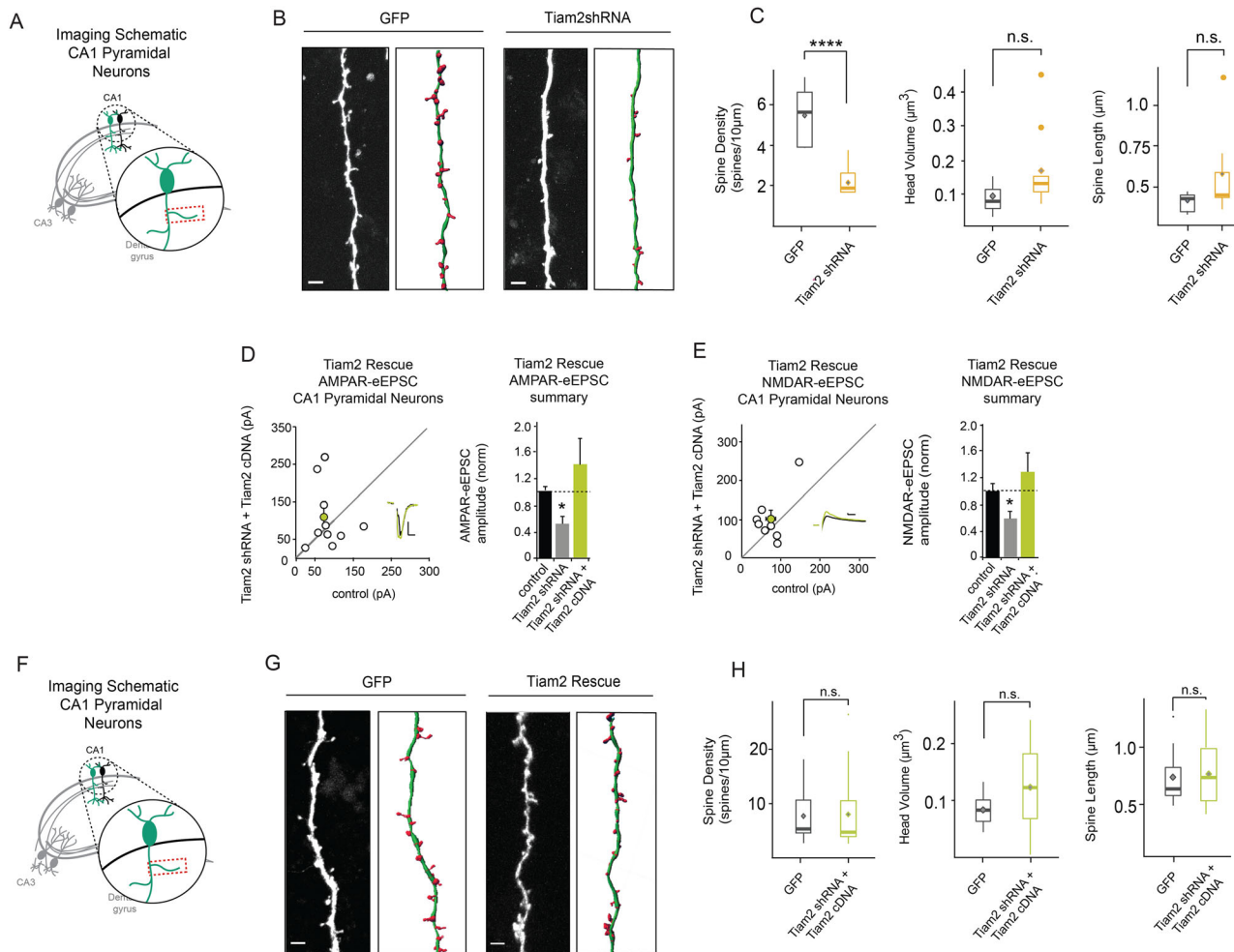
Figure 2. Tiam2 depletion results in reduced spine density in CA1 pyramidal neurons. ***A***, Schematic of areas of image acquisition from CA1 pyramidal neuron dendrites. ***B***, ***G***, Representative dendritic segments and corresponding reconstructed filaments (scale bars: 4 μm). ***C***, Boxplots show spine density is reduced in CA1 pyramidal neurons expressing Tiam2 shRNA (yellow) compared with GFP-expressing control neurons (gray; $p = 0.0000411$ for spine density; $p = 0.05031$ for spine head volume; $p = 0.22$ for spine length; for GFP $n = 9$ segments, $n = 6$ cells; for Tiam2 shRNA $n = 9$ segments, $n = 9$ cells; Wilcoxon rank-sum test). ***D***, ***E***, Scatterplots with AMPAR- and NMDAR-eEPSC amplitudes, respectively, plotted against paired control neuron eEPSCs (open circles) with $M \pm$ SEM (filled circles). (Insets) Representative current traces from control (black) and transfected (yellow) neurons with stimulation artifacts removed (scale bars: 20 pA for both AMPAR-eEPSCs and NMDAR-eEPSCs, 20 ms for AMPAR, 50 ms for NMDAR). Barplots show average AMPAR and NMDAR-eEPSC amplitudes (±SEM) of transfected CA1 pyramidal neurons normalized to respective control cell average eEPSC amplitudes (black). Tiam2 cDNA expression restores AMPAR- and NMDAR-eEPSC amplitude in CA1 pyramidal neurons coexpressing Tiam2 shRNA (for AMPAR-eEPSCs $p = 0.4$; $n = 9$ pairs; for NMDAR-eEPSC $p = 0.2$; $n = 8$ pairs; Wilcoxon signed-rank test). ***F***, Schematic of areas of image acquisition from CA1 pyramidal neuron dendrites. ***G***, ***H***, No significant differences were detected in any spine parameters in Tiam2 shRNA and Tiam2 cDNA coexpressing spines in CA1 pyramidal neurons compared with corresponding GFP-expressing control neurons. ***H***, Boxplots show unaltered spine density in CA1 pyramidal neurons expressing Tiam2 cDNA and Tiam2 shRNA (green) compared with GFP-expressing control neurons (gray boxes; $p = 0.7413$ for spine density; $p = 0.7376$ for spine head volume; $p = 0.5681$ for spine length; for GFP $n = 12$ segments, $n = 5$ cells; for Tiam2 shRNA $n = 16$ segments, $n = 11$ cells; Wilcoxon rank-sum test). ****$p < 0.0001$. See Extended Data Figure 2-1 for more details.

Prior evidence indicates Tiam1 expression is detected in DG granule neurons, which we confirmed (Extended Data Fig. 4-1A; Rao et al., 2019; Cheng et al., 2021). We wondered if Tiam1 could substitute for Tiam2 in CA1 pyramidal neurons. Neurons coexpressing Tiam2 shRNA and Tiam1 cDNA had glutamatergic neurotransmission comparable with control neurons (Fig. 4B,C), indicating that Tiam1 can substitute for Tiam2 function in neurotransmission at Schaffer collateral→CA1 pyramidal neuron synapses.

Having established Tiam2 is necessary for normal baseline neurotransmission at CA1 pyramidal neuron synapses; we tested whether Tiam2 affects mechanisms of synaptic plasticity. In acute mouse hippocampal slices where Tiam2 shRNA was delivered via in utero electroporation, we found Tiam2 depletion has no effect on the induction or maintenance of functional LTP at Schaffer collateral–CA1 pyramidal neurons (Fig. 4D). It is possible this lack of effect was due to a compensatory increase in Tiam1, but shRNA-mediated depletion does not affect expression of the either homolog in vitro (Extended Data Fig. 4-1B,C). Similarly, we found that Tiam1 knockdown produced no significant effect on LTP induction
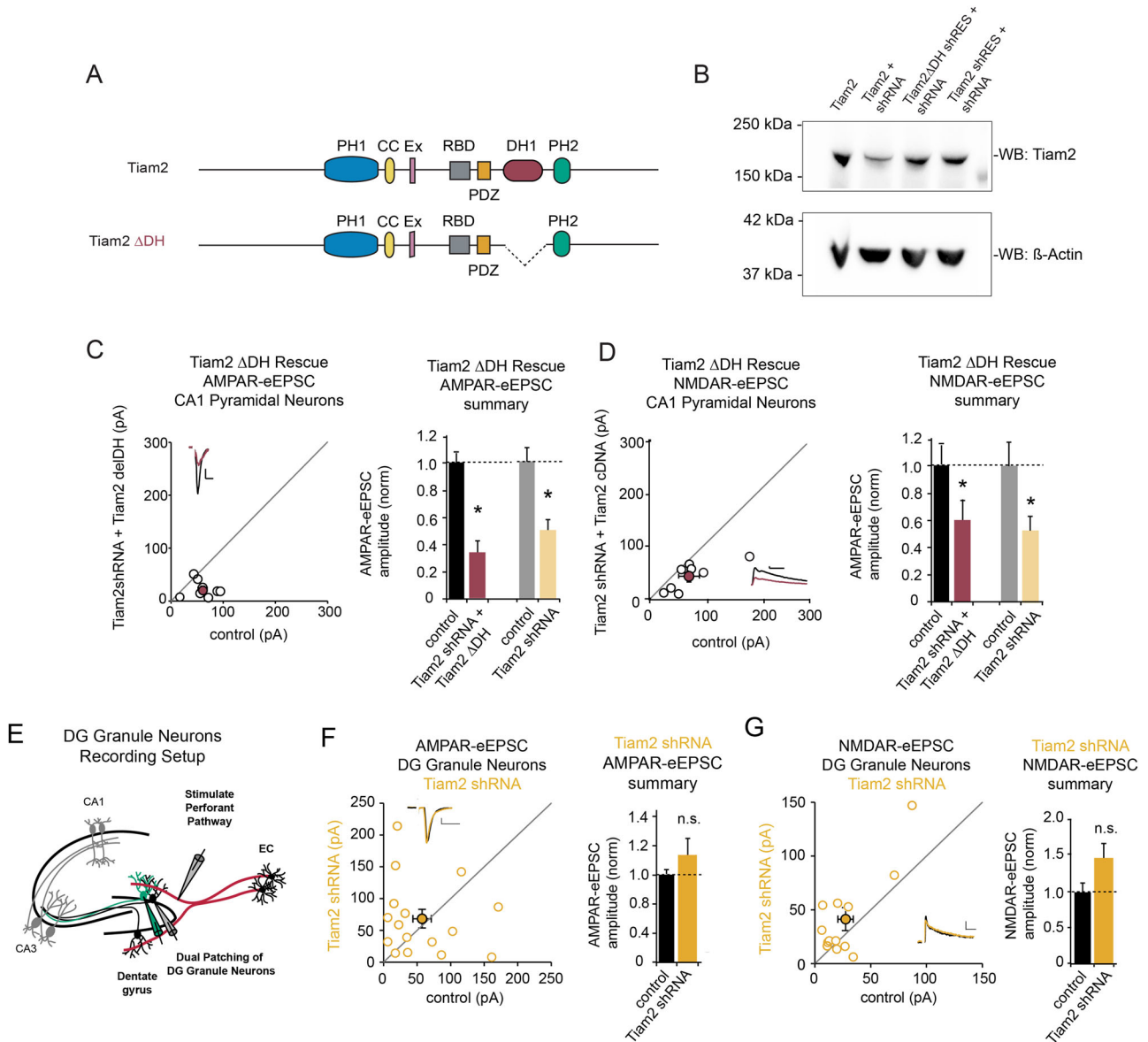
Figure 3. Tiam2 depletion is not rescued by DH1 domain-lacking Tiam2 in CA1 pyramidal neurons and has no effect on neurotransmission in DG granule neurons. ***A***, Illustration of Tiam2's protein domains; full-length Tiam2 (upper) and Tiam1 ΔDH (lower). ***B***, Immunoblot of shRNA-resistant Tiam2 ΔDH and Tiam2 cDNA coexpressed with Tiam2 shRNA in HEK293 cells. ***C***, ***D***, ***F***, ***G***, Scatterplots of AMPAR- and NMDAR-eEPSC amplitudes for CA1 pyramidal neurons expressing Tiam2 shRNA (yellow) and coexpressing Tiam2 shRNA and Tiam2 ΔDH (red), respectively, plotted against paired control neuron eEPSCs (open circles) with $M \pm SEM$ (filled circles). (Inset) Representative current traces from control (black) and transfected (yellow or red) neurons stimulation artifacts removed (scale bars: 20 pA for AMPA, 20 ms for AMPA). Barplots show average AMPAR and NMDAR-eEPSC amplitudes (±SEM) of transfected (yellow or red) CA1 pyramidal neurons normalized to respective control cell average eEPSC amplitudes (black). ***C***, ***D***, Tiam2 ΔDH does not restore AMPAR- and NMDAR-eEPSC amplitude in CA1 pyramidal neurons coexpressing Tiam2 shRNA (for AMPAR-eEPSCs $p = 0.016$, $n = 8$ pairs; for NMDAR-eEPSC $p = 0.016$, $n = 7$ pairs; Wilcoxon signed-rank test.). ***E***, Schematic representation of electrophysiological recording setup for DG granule neurons. ***F***, ***G***, Tiam2 knockdown has no effect on AMPAR- and NMDAR-eEPSC amplitude in DG granule neurons (for AMPAR-eEPSCs $p = 0.67$, $n = 16$ pairs; for NMDAR-eEPSC $p = 0.08$, $n = 13$ pairs; Wilcoxon signed-rank test) *$p < 0.05$, n.s., not significant. See Extended Data Figure 3-1 for more details.

or maintenance in CA1 pyramidal neurons (Fig. 4*E*), suggesting that neither Tiam2 nor Tiam1 individually plays an essential role in this form of synaptic plasticity at Schaffer collateral→CA1 pyramidal synapses.

Discussion

Loss-of-function studies describe the contribution of differential gene expression towards input-specific regulation of synaptic transmission and plasticity (Arnold and Heintz, 1997; Elias et al., 2008; Westerink et al., 2012). Here, we found the RhoGEF Tiam2 is essential for normal glutamatergic neurotransmission at Schaffer collateral→CA1 pyramidal neuron
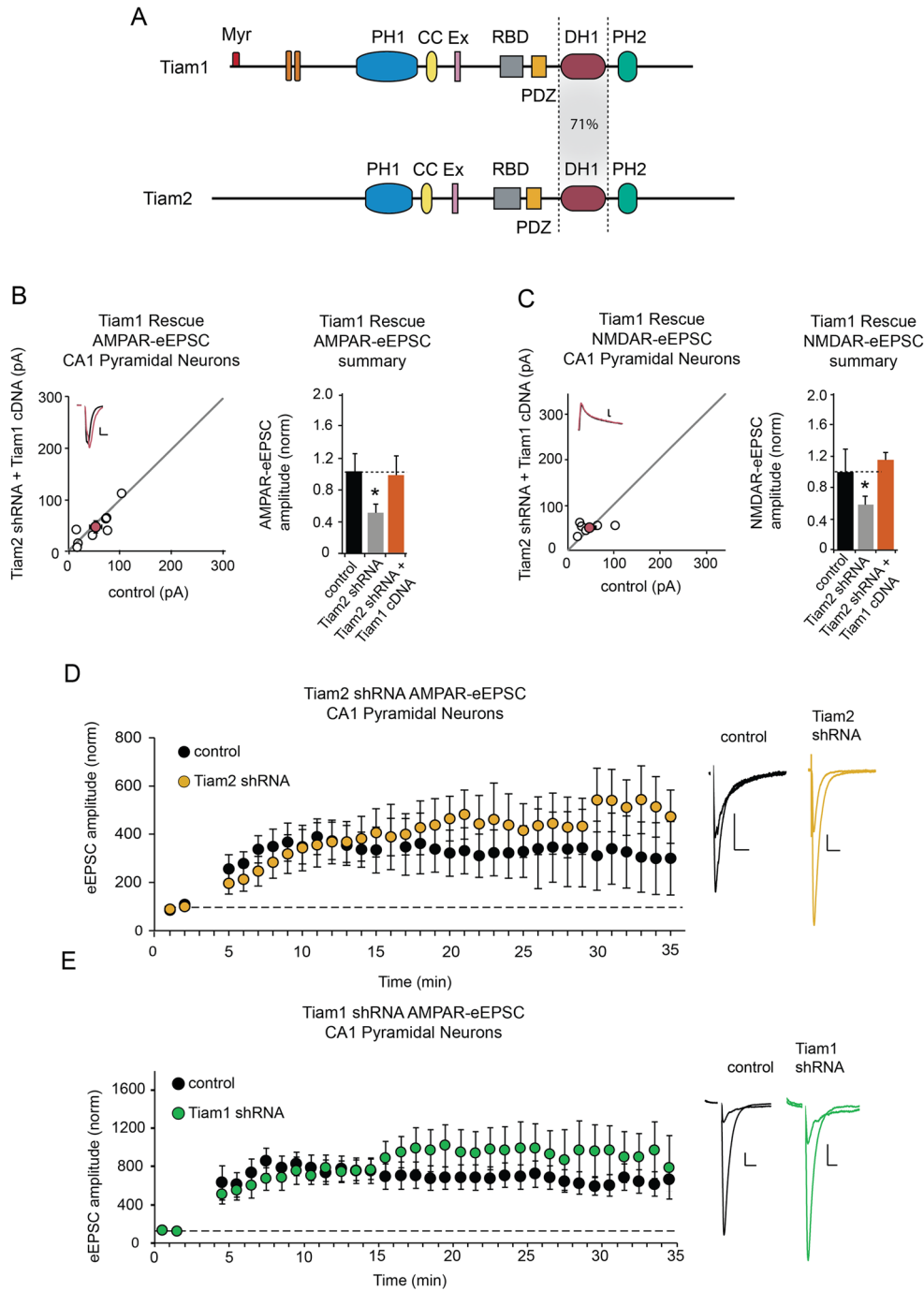
Figure 4. Tiam1 and Tiam2 are dispensable for functional LTP in CA1 pyramidal neurons. *A*, Illustration of Tiam1 and Tiam2 protein domains; full-length Tiam1 (upper) and Tiam2 (lower). *B*, *C*, Scatterplots with AMPAR- and NMDAR-eEPSC amplitudes for CA1 pyramidal neurons coexpressing Tiam2 shRNA and Tiam1 cDNA (orange), respectively, plotted against paired control neuron eEPSCs (open circles) with corresponding $M \pm SEM$ (filled circles). (Inset) Representative current traces from control (black) and transfected (green) neurons stimulation artifacts removed (scale bars: 20 pA for AMPA, 20 ms for AMPA). Barplots show average AMPAR and NMDAR-eEPSC amplitudes ($\pm$SEM) of CA1 pyramidal neurons normalized to respective control cell average eEPSC amplitudes (black bar). *B*, *C*, Tiam1 cDNA expression restores AMPAR- and NMDAR-eEPSC amplitude in CA1 pyramidal neurons coexpressing Tiam2 shRNA (for AMPAR-eEPSCs $p = 0.5$, $n = 8$ pairs; for NMDAR-eEPSC $p = 0.8$, $n = 6$ pairs, Wilcoxon signed-rank test; insets). *D*, *E*, LTP induction is unaltered by Tiam1 or Tiam2 depletion in CA1 pyramidal neurons. Plots of $M \pm SEM$ AMPAR-eEPSC amplitude of control untransfected CA1 pyramidal neurons (black) and CA1 pyramidal neurons electroporated with Tiam1shRNA (green) or Tiam2shRNA (yellow) normalized to the M AMPAR-eEPSC amplitude before an LTP induction protocol (arrow; Tiam1: control, $n = 9$ neurons; Tiam1shRNA, $n = 7$ neurons; Tiam2: control, $n = 9$ neurons; Tiam2 shRNA, $n = 7$ neurons). Sample AMPAR-eEPSC current traces from control (black) and electroporated (green or yellow) neurons before and after LTP induction are shown to the right of the graphs. (Scale bars: 20 ms, 20 pA.) *$p < 0.05$, Wilcoxon signed-rank test. See Extended Data Figure 4-1 for more details.

synapses. We show Tiam2 depletion in CA1 pyramidal neurons produces diminished synaptic currents conducted by postsynaptic glutamate receptors and that this depletion depends on the catalytic DH1 domain. Furthermore, Tiam2 depletion does not affect presynaptic glutamate release and reduces dendritic spine density, indicating that Tiam2 regulation of synapses is restricted to the postsynaptic compartment. Prior evidence indicates endogenous Tiam1 depletion does not affect baseline neurotransmission at Schaffer collateral→CA1 pyramidal neuron synapses (Rao et al., 2019). While we found recombinant Tiam1 rescues deficits from Tiam2 depletion at these synapses, differential ligand binding within other domains, PDZ or Pleckstrin homology coiled-coil extension (Zheng et al., 1996; Shepherd et al., 2011; Rao et al., 2019), may confer functional differences at other synapses. Tiam2 expression is evident within other hippocampal subregions. Surprisingly, Tiam2 depletion at perforant path–DG granule neurons produced no alterations in synaptic transmission. Overall, our analyses are consistent with necessary role of Tiam2 in the regulation of glutamatergic synapses in CA1 pyramidal neurons.

Several studies show Tiam1 is highly expressed in DG granule neurons (Ehler et al., 1997; Zhao et al., 2001; Lein et al., 2004, 2007; Rao et al., 2019; Cheng et al., 2021). This is consistent with our immunostaining of hippocampal slices (Extended Data Fig. 4-1*A*); however there are reports of Tiam1 expression in CA1 as well (Sasaki et al., 2010). We cannot rule out that Tiam1 plays a functional role in CA1 pyramidal neurons, but we find Tiam1 and Tiam2 are dispensable for functional LTP at Schaffer collateral→CA1 pyramidal neuron synapses. RhoGEFs Trio and Kalirin are required for the expression of LTP in CA1 pyramidal neurons (Herring and Nicoll, 2016). Since our experimental paradigm produces a depletion and does not eliminate protein expression, it is entirely possible that low levels of Tiam1 or Tiam2 protein, together with Trio and Kalirin, contribute to LTP in CA1 pyramidal neurons. Recent studies report a Tiam1-mediated deficit in structural synaptic plasticity in CA1 pyramidal neurons (Kojima et al., 2019; Saneyoshi et al., 2019), and structural and functional LTP are well correlated (Matsuzaki et al., 2004). Our data support a dispensable role for Tiam1 and Tiam2 in LTP. This discrepancy may be explained by a partial contribution to plasticity by Tiam1, a possible cell autonomous role, or a role for Tiam1 at entorhinal→CA1 pyramidal neuron synapses.

Members of the RhoGEF protein family are implicated in glutamatergic synaptic deficits associated with neurodevelopmental disorders (Volk et al., 2015; Katrancha et al., 2017), and recent exome-sequencing studies have identified autism and schizophrenia-associated de novo missense mutations in Tiam1 and Tiam2 (Need et al., 2012; Takata et al., 2013; S. Lu et al., 2022). We show that Tiam2 is critical for glutamatergic synapse function at Schaffer collateral–CA1 pyramidal neurons. Additional RhoGEF proteins, such as Kalirin, Trio, and β-PIX, have been shown to have similar roles in supporting glutamatergic synapses in these neurons (Herring and Nicoll, 2016). This, along with the data from this study, suggests that Tiam2, Trio, and Kalirin form a cohort of RhoGEFs that are together responsible for normal glutamatergic neurotransmission at CA1 pyramidal neuron synapses. An improved understanding of their role in synapse development and function could contribute to therapeutics for neurodevelopmental disorders.

References

Arnold DB, Heintz N (1997) A calcium responsive element that regulates expression of two calcium binding proteins in Purkinje cells. Proc Natl Acad Sci U S A 94:8842–8847.

Bekkers JM, Stevens CF (1990) Presynaptic mechanism for long-term potentiation in the hippocampus. Nature 346:724–729.

Bonnici B, Kapfhammer JP (2009) Modulators of signal transduction pathways can promote axonal regeneration in entorhino-hippocampal slice cultures. Eur J Pharmacol 612:35–40.

Cembrowski MS, Wang L, Sugino K, Shields BC, Spruston N (2016) Hipposeq: a comprehensive RNA-seq database of gene expression in hippocampal principal neurons. Elife 5:e14997.

Chan Y-L, Lai W-C, Chen J-S, Tseng JT-C, Chuang P-C, Jou J, Lee C-T, Sun HS (2020) TIAM2S mediates serotonin homeostasis and provokes a pro-inflammatory immune microenvironment permissive for colorectal tumorigenesis. Cancers 12:1844.

Cheng J, et al. (2021) The Rac-GEF Tiam1 promotes dendrite and synapse stabilization of dentate granule cells and restricts hippocampal-dependent memory functions. J Neurosci 41:1191–1206.

Chiu C-Y, Leng S, Martin KA, Kim E, Gorman S, Duhl DMJ (1999) Cloning and characterization of T-cell lymphoma invasion and metastasis 2 (TIAM2), a novel guanine nucleotide exchange factor related to TIAM1. Genomics 61:66–73.

Cook DR, Rossman KL, Der CJ (2014) Rho guanine nucleotide exchange factors: regulators of Rho GTPase activity in development and disease. Oncogene 33:4021–4035.

Del Castillo J, Katz B (1954) Quantal components of the end-plate potential. J Physiol 124:560–573.

Ehler E, van Leeuwen F, Collard JG, Salinas PC (1997) Expression of Tiam-1 in the developing brain suggests a role for the Tiam-1-Rac signaling pathway in cell migration and neurite outgrowth. Mol Cell Neurosci 9:1–12.

Elias GM, Elias LA, Apostolides PF, Kriegstein AR, Nicoll RA (2008) Differential trafficking of AMPA and NMDA receptors by SAP102 and PSD-95 underlies synapse development. Proc Natl Acad Sci U S A 105:20953–20958.

Farris S, Ward JM, Carstens KE, Samadi M, Wang Y, Dudek SM (2019) Hippocampal subregions express distinct dendritic transcriptomes that reveal differences in mitochondrial function in CA2. Cell Rep 29:522–539.e6.

Fort P, Blangy A (2017) The evolutionary landscape of Dbl-Like RhoGEF families: adapting eukaryotic cells to environmental signals. Genome Biol Evol 9:1471–1486.

Franjic D, et al. (2022) Transcriptomic taxonomy and neurogenic trajectories of adult human, macaque, and pig hippocampal and entorhinal cells. Neuron 110:452–469.e14.

Fu WY, et al. (2007) Cdk5 regulates EphA4-mediated dendritic spine retraction through an ephexin1-dependent mechanism. Nat Neurosci 10:67–76.

Gerber KJ, Dammer EB, Duong DM, Deng Q, Dudek SM, Seyfried NT, Hepler JR (2019) Specific proteomes of hippocampal regions CA2 and CA1 reveal proteins linked to the unique physiology of area CA2. J Proteome Res 18:2571–2584.

Goto A, Hoshino M, Matsuda M, Nakamura T (2011) Phosphorylation of STEF/Tiam2 by protein kinase A is critical for Rac1 activation

and neurite outgrowth in dibutyryl cAMP–treated PC12D cells. Mol Biol Cell 22:1780–1790.

Gray JA, Shi Y, Usui H, During MJ, Sakimura K, Nicoll RA (2011) Distinct modes of AMPA receptor suppression at developing synapses by GluN2A and GluN2B: single-cell NMDA receptor subunit deletion in vivo. Neuron 71:1085–1101.

Gutman-Wei AY, Brown SP (2021) Mechanisms underlying target selectivity for cell types and subcellular domains in developing neocortical circuits. Front Neural Circuits 15:728832.

Hamilton AM, Lambert JT, Parajuli LK, Vivas O, Park DK, Stein IS, Jahncke JN, Greenberg ME, Margolis SS, Zito K (2017) A dual role for the RhoGEF Ephexin5 in regulation of dendritic spine outgrowth. Mol Cell Neurosci 80:66–74.

Herring BE, Nicoll RA (2016) Kalirin and Trio proteins serve critical roles in excitatory synaptic transmission and LTP. Proc Natl Acad Sci U S A 113:2264.

Hoshino M, Sone M, Fukata M, Kuroda S, Kaibuchi K, Nabeshima Y, Hama C (1999) Identification of the stef gene that encodes a novel guanine nucleotide exchange factor specific for Rac1. J Biol Chem 274:17837–17844.

Incontro S, Díaz-Alonso J, Iafrati J, Vieira M, Asensio CS, Sohal VS, Roche KW, Bender KJ, Nicoll RA (2018) The CaMKII/NMDA receptor complex controls hippocampal synaptic transmission by kinase-dependent and independent mechanisms. Nat Commun 9:2069.

Kang H, Schuman EM (1995) Long-lasting neurotrophin-induced enhancement of synaptic transmission in the adult hippocampus. Science 267:1658–1662.

Karnoub AE, Worthylake DK, Rossman KL, Pruitt WM, Campbell SL, Sondek J, Der CJ (2001) Molecular basis for Rac1 recognition by guanine nucleotide exchange factors. Nat Struct Biol 8:1037–1041.

Katrancha SM, Wu Y, Zhu M, Eipper BA, Koleske AJ, Mains RE (2017) Neurodevelopmental disease-associated de novo mutations and rare sequence variants affect TRIO GDP/GTP exchange factor activity. Hum Mol Genet 26:4728–4740.

Ke MT, Fujimoto S, Imai T (2013) SeeDB: a simple and morphology-preserving optical clearing agent for neuronal circuit reconstruction. Nat Neurosci 16:1154–1161.

Kojima H, Rosendale M, Sugiyama Y, Hayashi M, Horiguchi Y, Yoshihara T, Ikegaya Y, Saneyoshi T, Hayashi Y (2019) The role of CaMKII-Tiam1 complex on learning and memory. Neurobiol Learn Mem 166:107070.

Kokaia M, Asztely F, Olofsdotter K, Sindreu CB, Kullmann DM, Lindvall O (1998) Endogenous neurotrophin-3 regulates short-term plasticity at lateral perforant path–granule cell synapses. J Neurosci 18:8730–8739.

Lein ES, Zhao X, Gage FH (2004) Defining a molecular atlas of the hippocampus using DNA microarrays and high-throughput in situ hybridization. J Neurosci 24:3879–3889.

Lein ES, et al. (2007) Genome-wide atlas of gene expression in the adult mouse brain. Nature 445:168–176.

Levy JM, Chen X, Reese TS, Nicoll RA (2015) Synaptic consolidation normalizes AMPAR quantal size following MAGUK loss. Neuron 87:534–548.

Lu S, et al. (2022) Loss-of-function variants in TIAM1 are associated with developmental delay, intellectual disability, and seizures. Am J Hum Genet 109:571–586.

Lu W, Shi Y, Jackson AC, Bjorgan K, During MJ, Sprengel R, Seeburg PH, Nicoll RA (2009) Subunit composition of synaptic AMPA receptors revealed by a single-cell genetic approach. Neuron 62:254–268.

Malinow R, Tsien RW (1990) Presynaptic enhancement shown by whole-cell recordings of long-term potentiation in hippocampal slices. Nature 346:177–180.

Marcassa G, Dascenco D, de Wit J (2023) Proteomics-based synapse characterization: from proteins to circuits. Curr Opin Neurobiol 79:102690.

Margolis SS, et al. (2010) EphB-mediated degradation of the RhoA GEF Ephexin5 relieves a developmental brake on excitatory synapse formation. Cell 143:442–455.

Martin-Vilchez S, Whitmore L, Asmussen H, Zareno J, Horwitz R, Newell-Litwa K (2017) RhoGTPase regulators orchestrate distinct stages of synaptic development. PLoS One 12:e0170464.

Matsuo N, Hoshino M, Yoshizawa M, Nabeshima Y (2002) Characterization of STEF, a guanine nucleotide exchange factor for Rac1, required for neurite growth. J Biol Chem 277:2860–2868.

Matsuzaki M, Honkura N, Ellis-Davies GCR, Kasai H (2004) Structural basis of long-term potentiation in single dendritic spines. Nature 429:761–766.

McAllister AK (2004) Biolistic transfection of cultured organotypic brain slices. Methods Mol Biol 245:197–206.

Miller MB, Yan Y, Eipper BA, Mains RE (2013) Neuronal Rho GEFs in synaptic physiology and behavior. Neuroscientist 19:255–273.

Need AC, et al. (2012) Exome sequencing followed by large-scale genotyping suggests a limited role for moderately rare risk factors of strong effect in schizophrenia. Am J Hum Genet 91:303–312.

Penzes P, Johnson RC, Sattler R, Zhang X, Huganir RL, Kambampati V, Mains RE, Eipper BA (2001) The neuronal Rho-GEF kalirin-7 interacts with PDZ domain-containing proteins and regulates dendritic morphogenesis. Neuron 29:229–242.

Penzes P, Beeser A, Chernoff J, Schiller MR, Eipper BA, Mains RE, Huganir RL (2003) Rapid induction of dendritic spine morphogenesis by trans-synaptic ephrinB-EphB receptor activation of the Rho-GEF kalirin. Neuron 37:263–274.

Pfeiffer BE, Zang T, Wilkerson JR, Taniguchi M, Maksimova MA, Smith LN, Cowan CW, Huber KM (2010) Fragile X mental retardation protein is required for synapse elimination by the activity-dependent transcription factor MEF2. Neuron 66:191–197.

Prang P, Del Turco D, Kapfhammer JP (2001) Regeneration of entorhinal fibers in mouse slice cultures is age dependent and can be stimulated by NT-4, GDNF, and modulators of G-proteins and protein kinase C. Exp Neurol 169:135–147.

Rao S, Kay Y, Herring BE (2019) Tiam1 is critical for glutamatergic synapse structure and function in the hippocampus. J Neurosci 39:9306.

Saneyoshi T, Matsuno H, Suzuki A, Murakoshi H, Hedrick NG, Agnello E, O'Connell R, Stratton MM, Yasuda R, Hayashi Y (2019) Reciprocal activation within a kinase-effector complex underlying persistence of structural LTP. Neuron 102:1199–1210.e96.

Sasaki N, Kurisu J, Kengaku M (2010) Sonic hedgehog signaling regulates actin cytoskeleton via Tiam1–Rac1 cascade during spine formation. Mol Cell Neurosci 45:335–344.

Schnell E, Sizemore M, Karimzadegan S, Chen L, Bredt DS, Nicoll RA (2002) Direct interactions between PSD-95 and stargazin control synaptic AMPA receptor number. Proc Natl Acad Sci U S A 99:13902–13907.

Shepherd TR, Hard RL, Murray AM, Pei D, Fuentes EJ (2011) Distinct ligand specificity of the Tiam1 and Tiam2 PDZ domains. Biochemistry 50:1296–1308.

Stoppini L, Buchs PA, Muller D (1991) A simple method for organotypic cultures of nervous tissue. J Neurosci Methods 37:173–182.

Takata A, et al. (2013) A population-specific uncommon variant in GRIN3A associated with schizophrenia. Biol Psychiatry 73:532–539.

Tashiro A, Yuste R (2004) Regulation of dendritic spine motility and stability by Rac1 and Rho kinase: evidence for two forms of spine motility. Mol Cell Neurosci 26:429–440.

Volk L, Chiu SL, Sharma K, Huganir RL (2015) Glutamate synapses in human cognitive disorders. Annu Rev Neurosci 38:127–149.

Westerink RH, Beekwilder JP, Wadman WJ (2012) Differential alterations of synaptic plasticity in dentate gyrus and CA1 hippocampal area of calbindin-D28K knockout mice. Brain Res 1450:1–10.

Wichmann C, Kuner T (2022) Heterogeneity of glutamatergic synapses: cellular mechanisms and network consequences. Physiol Rev 102:269–318.

Worthylake DK, Rossman KL, Sondek J (2000) Crystal structure of Rac1 in complex with the guanine nucleotide exchange region of Tiam1. Nature 408:682–688.

Yoshizawa M, Hoshino M, Sone M, Nabeshima Y-I (2002) Expression of stef, an activator of Rac1, correlates with the stages of neuronal

morphological development in the mouse brain. Mech Dev 113:65–68.

Zhao X, Lein ES, He A, Smith SC, Aston C, Gage FH (2001) Transcriptional profiling reveals strict boundaries between hippocampal subregions. J Comp Neurol 441:187–196.

Zheng Y, Zangrilli D, Cerione RA, Eva A (1996) The pleckstrin homology domain mediates transformation by oncogenic Dbl through specific intracellular targeting*. J Biol Chem 271:19017–19020.

Zhu F, et al. (2018) Architecture of the mouse brain synaptome. Neuron 99:781–799.e10.